Supplementary Information for: The Simulation of X-ray Absorption Spectra Including Vibronic Coupling: Application of the QD-DFT/MRCI(2) Method†

Martha Yaghoubi Jouybari,[1] Simon P. Neville,[2] and Michael S. Schuurman[2,1,*]

[1]*Department of Chemistry and Biomolecular Sciences, University of Ottawa, 10 Marie Curie, Ottawa, Ontario, K1N 6N5, Canada*

[2]*National Research Council Canada, 100 Sussex Drive, Ottawa, Ontario K1A 0R6, Canada*

(Dated: October 3, 2025)

WAVE PACKET PROPAGATIONS

Standard approaches achieve numerically exact solutions by representing the wavepacket as a linear combination of time-independent basis functions (usually one-dimensional). Each basis function has a time-dependent coefficient that captures the wavepacket's evolution[2, 5, 16].

$$\Psi(q,t) = \sum_{j_1 \cdots j_f} A_{j_1 \cdots j_f}(t) \chi_{j_1}^{(1)}(q_1) \ldots \chi_{j_f}^{(f)}(q_f) \tag{1}$$

where $\chi_{j_\kappa}^{(\kappa)}(q_\kappa)$ are the set of 1D orthogonal basis functions for the κth degree of freedom(DOF) and $A_{j_1 \cdots j_f}(t)$ the time-dependent expansion coefficients which are obtained by using a variational method equations of motion[3, 6].

The Multiconfiguration Time-Dependent Hartree (MCTDH) method provides an efficient approach to obtain $\Psi(q,t)$ by expanding the wavefunction in a time-dependent basis set (φ^κ), called single-particle functions (SPFs)[1, 9, 11].

$$\Psi(q,t) = \sum_{j_1 \cdots j_f} A_{j_1 \cdots j_f}(t) \varphi_{j_1}^{(1)}(Q_1,t) \ldots \varphi_{j_f}^{(f)}(Q_f,t) \tag{2}$$

The time-dependent single-particle functions (SPFs) are further expanded in a time-independent basis set constructed using a discrete variable representation (DVR). A key advantage of MCTDH is its use of mode combination, allowing the use of low-dimensional SPFs based on combined or logical coordinates(Q_κ), which improves efficiency[4, 17].

$$Q_\kappa = (q_1^\kappa, q_2^\kappa, ..., q_d^\kappa) \tag{3}$$

While combining modes significantly enhances MCTDH efficiency compared to standard methods, it becomes increasingly challenging to propagate larger combined SPFs in larger systems. Fortunately, we can leverage the strengths of MCTDH itself to address this bottleneck. This is the core idea behind the Multilayer Multiconfiguration Time-Dependent Hartree (ML-MCTDH) approach. Instead of directly propagating increasingly complex SPFs, ML-MCTDH employs a recursive strategyin which multiconfigurational ansatz is used for the multidimensional SPFs of an underlying MCTDH expansion[8, 10, 13–16].

For quantum dynamics simulations of the ethylene molecule, the standard multi-configurational time-dependent Hartree (MCTDH) method with mode combination was employed. For more complex molecules, allene and butadiene, a matrix product state (MPS)-type wave function ansatz implemented within the ML-MCTDH framework was employed. The MPS approaches are a compact and highly efficient representation of wave functions in high-dimensional systems, by decomposing the wave function into a network of low-rank tensors.

Similarly to the ML-MCTDH approach, the starting point for the MPS-based method for wavepacket propagation is to expand the d-dimensional wave function, $\Psi(Q_1, Q_2, ..., Q_d, t)$, in terms of one-dimensional discrete variable representation (DVR) basis functions, $\chi_i^{(\kappa)}(Q_\kappa)$, for each degree of freedom:

$$\Psi(Q_1, Q_2, ..., Q_d, t) = \sum_{i_1=1}^{N_1} ... \sum_{i_d=1}^{N_d} C_{i_1,...,i_d}(t) \chi_{i_1}^{(1)}(Q_1) ... \chi_{i_d}^{(d)}(Q_d) \tag{4}$$

However, analogously to the MCTDH formulation, the time-dependent coefficient tensor,$\mathbf{C}(t) \in \mathbb{C}^{N_1 \times \cdots \times N_d}$, scales exponentially with the number of degrees of freedom, making direct propagation computationally intractable for larger systems. To address this, the time-dependent coefficient tensor is then further expanded using a MPS decomposition, where the full coefficient tensor is expressed as a sequential product of lower-rank tensors,r_κ:

$$C_{i_1,...,i_d}(t) = \sum_{\{\alpha_k\}} A^{(1)}_{\alpha_0,i_1,\alpha_1}(t)\, A^{(2)}_{\alpha_1,i_2,\alpha_2}(t) \cdots A^{(d)}_{\alpha_{d-1},i_d,\alpha_d}(t) \tag{5}$$

Similarly to the Ml strategy in ML-MCTDH, each MPS tensor is factorized into a product of two smaller tensors,$\mathbf{b}^{(\kappa)}(t) \in \mathbb{C}^{r_{\kappa-1} \times s_\kappa \times r_\kappa}$ and $\mathbf{c}^{(\kappa)}(t) \in \mathbb{C}^{s_\kappa \times N_\kappa}$:

$$A^{(\kappa)}_{\alpha_{\kappa-1},i_\kappa,\alpha_\kappa}(t) = \sum_{\beta=1}^{s_\kappa} b^{(\kappa)}_{\alpha_{\kappa-1},\beta,\alpha_\kappa}(t)\, c^{(\kappa)}_{\beta,i_\kappa}(t) \tag{6}$$

The MCTDH operator files (*.op) that fully define the vibronic Hamiltonian employed for each molecule are included separately.

Table S1. Mathematical form of the diabatic potential matrix $W_{ij}(\mathbf{Q})$ for different models.

Model	Expression for $W_{ij}(\mathbf{Q})$
Adiabatic Anharmonic (AA)	$W_{ij}^{\mathrm{AA}}(\mathbf{Q}) \approx \tau_0^{(i,j)} + \sum_{p=1}^{6} \frac{1}{p!} \sum_{\alpha=1}^{d} \tau_{p\alpha}^{(i,i)} Q_\alpha^p$
1D Non-Adiabatic (1D-NA)	$W_{ij}^{\text{1D-NA}}(\mathbf{Q}) \approx \tau_0^{(i,j)} + \sum_{p=1}^{6} \frac{1}{p!} \sum_{\alpha=1}^{d} \tau_{p\alpha}^{(i,j)} Q_\alpha^p$
Full Non-Adiabatic (NA)	$W_{ij}^{\mathrm{NA}}(\mathbf{Q}) \approx \tau_0^{(i,j)} + \sum_{p=1}^{6} \frac{1}{p!} \sum_{\alpha=1}^{d} \tau_{p\alpha}^{(i,j)} Q_\alpha^p + \frac{1}{2} \sum_{\alpha,\beta=1}^{d} \eta_{\alpha\beta}^{(i,j)} Q_\alpha Q_\beta$

VIBRONIC SPECTRA CALCULATION

Ethylene

Electronic structure Calculation

```
Geometry information of ethylenee
C      0.0000000     0.0000000     0.0000000
C      0.0000000     0.0000000     1.3004180
C      0.0000000     0.0000000    -1.3004181
H      0.0000000     0.9258140     1.8632318
H      0.0000000    -0.9258140     1.8632318
H      0.9258140     0.0000000    -1.8632318
H     -0.9258140     0.0000000    -1.8632318
```

States	Computed f_i	Adjusted f_i	Computed E_i^0 (eV)	Energy Shifts (eV)
$1B_{1u}$	0.098	0.098	285.11	-0.25
$1B_{3u}$	0.009	0.009	286.89	0.4
$1B_{2u}$	0.028	0.028	287.52	0.4
$2B_{3u}$	0.001	0.001	287.60	0.15
$2B_{1u}$	0.010	0.010	288.43	0.15
$2B_{2u}$	0.005	0.005	288.60	0.15
$3B_{3u}$	0.0002	0.0002	288.94	0.15
$4B_{3u}$	0.013	0.026	289.66	-0.05
$3B_{2u}$	0.025	0.050	289.79	-0.05
$5B_{3u}$	0.001	0.002	289.89	-0.05
$3B_{1u}$	0.007	0.014	289.94	-0.05
$6B_{3u}$	0.0	0.0	290.37	-0.05

Table S2. Computed and adjusted oscillator strengths (f_i) for ethylene, along with the applied energy shifts. The computed values are obtained from electronic structure calculations, while the adjusted values are modified to improve agreement with experimental spectra. The Energy Shifts column reflects the applied corrections to the computed excitation energies, yielding empirically informed theoretical best estimates of the vertical excitation energies (ϵ_{0i}).

normal mode	Operator File Label
$Q1$	$Q10$
$Q2$	$Q8$
$Q3$	$Q6$
$Q4$	$Q4$
$Q5$	$Q11$
$Q6$	$Q5$
$Q7$	$Q2$
$Q8$	$Q3$
$Q9$	$Q12$
$Q10$	$Q1$
$Q11$	$Q9$
$Q12$	$Q7$

Table S3. Mapping of normal mode labels used in the operator files of ethylene.

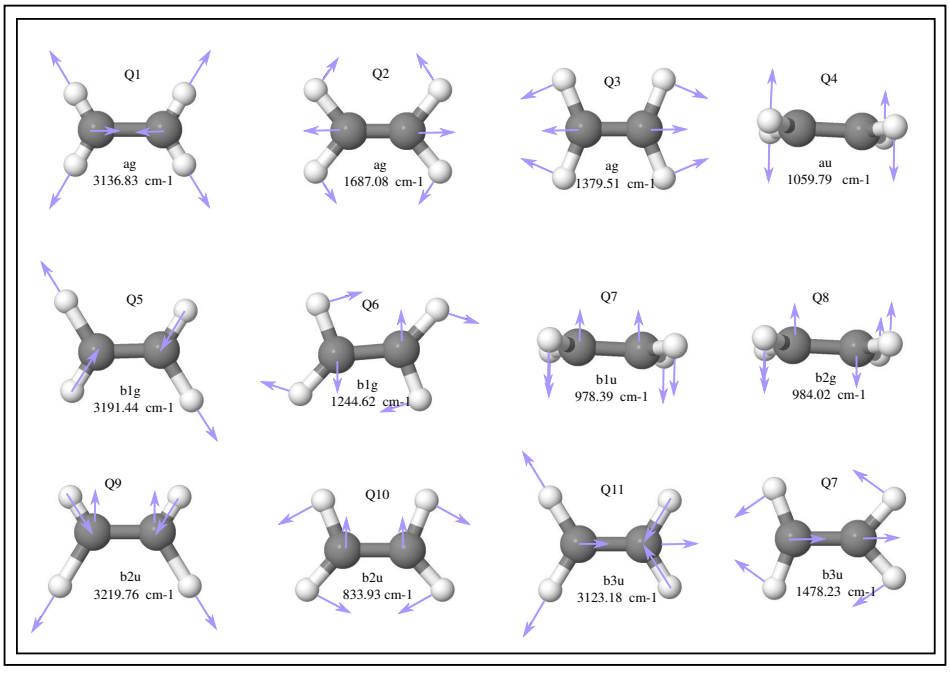

Figure S1. Vibrational normal modes of ethylene

Excitation Energies and Character

Spectra

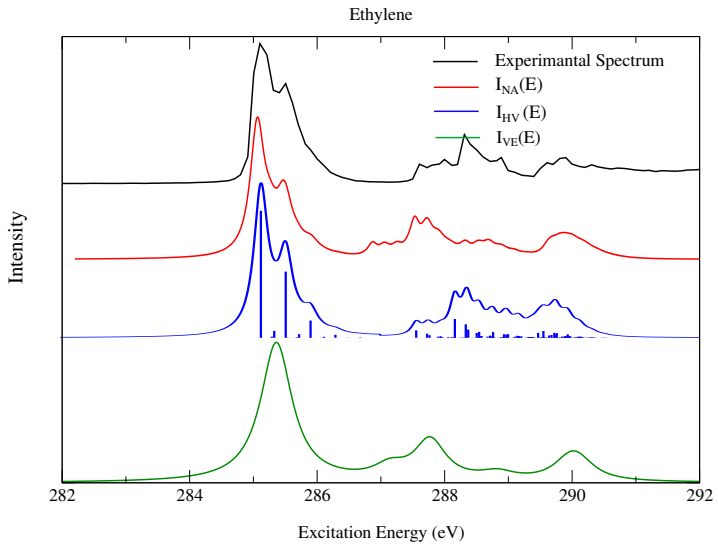

Figure S2. The experimental X-ray absorption of ethylene compared to simulations without shifting excitation energy of each core-excited state in the calculated spectra performed employing a hierarchy of approximations. From bottom, the I_{VE} is a purely electronic spectrum employing vertical excitation energies and oscillator strengths only (green line), I_{HV} is poisson distribution spectrum corresponding to vibrational structure arising from treating the excited states as a series of displaced harmonic oscillators (blue line), and I_{NA}, the full non-adiabatic vibronic coupling simulation (red line). The experimental spectrum is at top (black line). [7].

The contributions of individual transitions to the total spectrum are illustrated in Figure S5. Our simulations indicate that the prominent spectral feature centered at 285 eV is attributed to the dipole-allowed C $1s \rightarrow \pi^*$ transition. The spectral region between 287 and 290 eV exhibits a more complex structure as a result of overlapping contributions from multiple states. But, overall speaking, the peaks above 287 eV are generally attributed to C $1s$ Rydberg transitions.

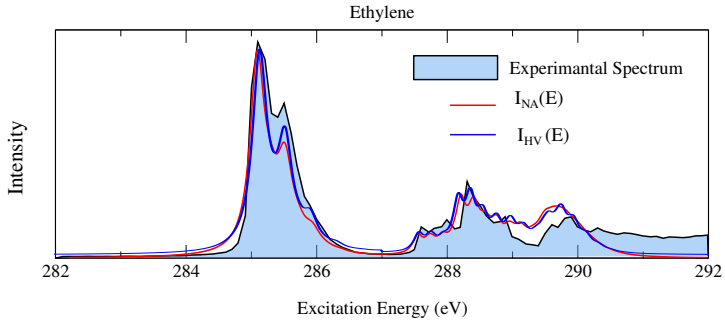

Figure S3. Comparison of computed X-ray absorption spectra of ethylene to assess the effect of vibronic coupling on the total absorption spectra. Spectra were calculated using the poisson distribution spectrum (blue line) and the the full non-adiabatic vibronic coupling simulation (red line). The shaded area represents the experimental spectrum, shown for comparison [7].

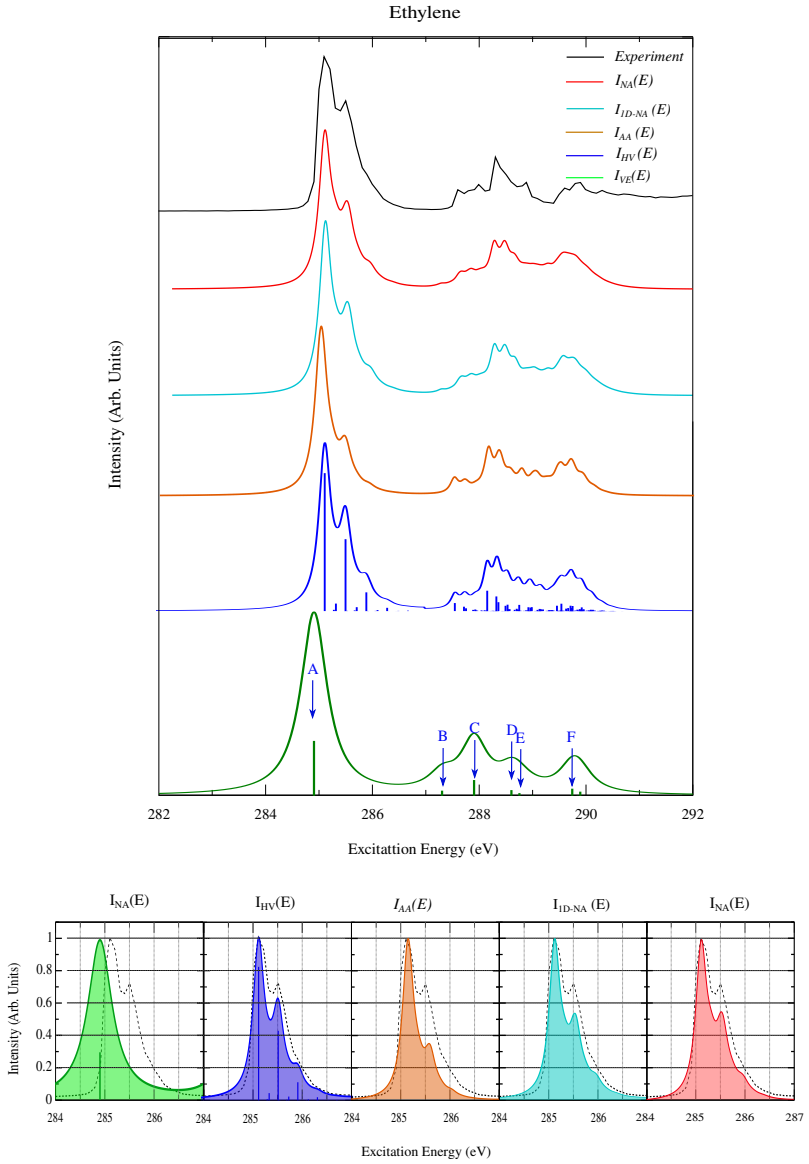

Figure S4. The experimental X-ray absorption of ethylene compared to simulations performed employing a hierarchy of approximations. From bottom, the I_{VE} is a purely electronic spectrum employing vertical excitation energies and oscillator strengths only (green line), I_{HV} is poisson distribution spectrum corresponding to vibrational structure arising from treating the excited states as a series of displaced harmonic oscillators (blue line), I_{AA}, the vibronic coupling Hamiltonian model considering only one-mode terms for the diabatic potential and all interstate couplings were switched off (orange line), I_{1D-NA}, the vibronic coupling Hamiltonian model considering only one-mode terms for the diabatic potential and inter-state coupling terms, and I_{NA}, the full non-adiabatic vibronic coupling simulation (red line). The experimental spectrum is at top (black line). [7]. The bottom panels evince a detailed comparison of the various approximations with the experimental band origin.

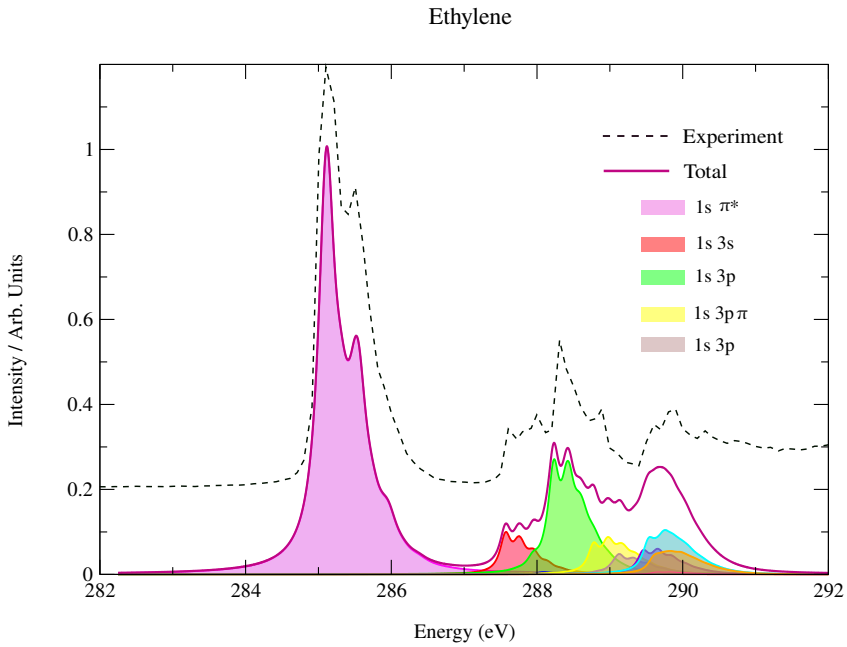

Figure S5. Vibronic absorption spectra of ethylene including individual state component computed using vibronic coupling Hamiltonians parameterized via fitting to quasi-diabatic potentials computed at the QD-DFT/MRCI(2) levels of theory using the aug-cc-pVTZ basis.

Allene

Geometry and Normal Modes

```
Geometry information of Allene

C      0.0000000     0.0000000     0.0000000
C      0.0000000     0.0000000     1.3004154
C      0.0000000     0.0000000    -1.3004154
H      0.6546490     0.6546490     1.8632299
H     -0.6546490    -0.6546490     1.8632299
H      0.6546490    -0.6546490    -1.8632299
H     -0.6546490     0.6546490    -1.8632299
```

Allene, in its equilibrium configuration, belongs to the D_{2d} point group, whose character table includes the irreducible representations A_1, A_2, B_1, B_2 and E. DFT-MRCI calculations were performed using the C_{2v} subgroup of D_{2d}, as these calculations require Abelian point groups. The C_{2v} point group has irreducible representations of A_1, A_2, B_1, B_2. Consequently, the symmetry assignments of the vibrational normal modes differ between the D_{2d} and C_{2v} point groups. Furthermore, the spectroscopic ordering of the normal modes differs from the ordering used in the operator files for the simulations. Table 3 provides a mapping between the symmetry labels of the normal modes in the two point groups and the corresponding labels used in the operator files.

States	Computed f_i	Adjusted f_i	Computed E_i^0 (eV)	Energy Shifts (eV)
$1B_1$	0.0564	0.0564	285.63	-0.05
$1B_2$	0.0564	0.0564	285.63	-0.05
$2B_2$	0.0417	0.0417	285.74	0.05
$2B_1$	0.0417	0.0417	285.74	0.05
$3B_1$	0.0055	0.0110	286.61	-0.05
$3B_2$	0.0055	0.0110	286.61	-0.05
$2A_1$	0.0044	0.0088	286.98	0.25
$4A_1$	0.0066	0.0132	287.76	0.05
$4B_1$	0.0073	0.0146	288.16	0.35
$4B_2$	0.0073	0.0146	288.16	0.35
$5B_1$	0.0067	0.0134	288.25	0.35
$5B_2$	0.0067	0.0134	288.25	0.35
$7B_1$	0.0024	0.0048	289.18	0.35
$7B_2$	0.0024	0.0048	289.18	0.35

Table S4. Computed and adjusted oscillator strengths (f_i) for allene, along with the applied energy shifts. The computed values are obtained from electronic structure calculations, while the adjusted values are modified to improve agreement with experimental spectra. The Energy Shifts column reflects the applied corrections to the computed excitation energies, yielding empirically informed theoretical best estimates of the vertical excitation energies (ϵ_{0i}).

normal mode	Symmetry in D_{2d}	Symmetry in C_{2v}	Operator File Label
$Q1$	a_1	a_1	$Q13$
$Q2$	a_1	a_1	$Q9$
$Q3$	a_1	a_1	$Q8$
$Q4$	b_1	a_2	$Q5$
$Q5$	b_2	a_1	$Q12$
$Q6$	b_2	a_1	$Q11$
$Q7$	b_2	a_1	$Q10$
$Q8_x$	e	b_2	$Q14$
$Q8_y$	e	b_1	$Q15$
$Q9_x$	e	b_1	$Q16$
$Q9_y$	e	b_2	$Q17$
$Q10_x$	e	b_2	$Q1$
$Q10_y$	e	b_1	$Q2$
$Q11_x$	e	b_2	$Q3$
$Q11_y$	e	b_1	$Q4$

Table S5. Mapping of normal mode symmetries between D_{2d} and C_{2v} point groups, along with the labels used in the operator files of allene.

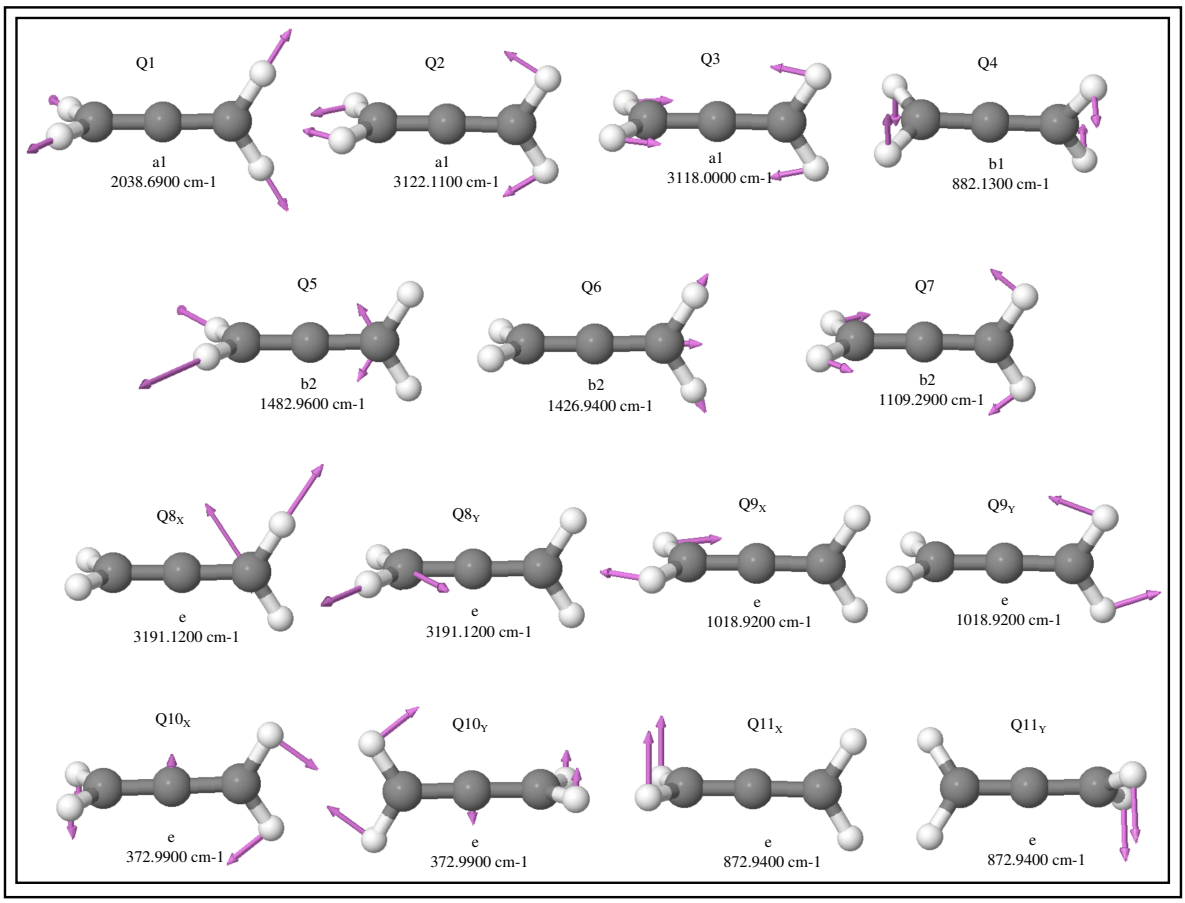

Figure S6. Vibrational normal modes of allene.

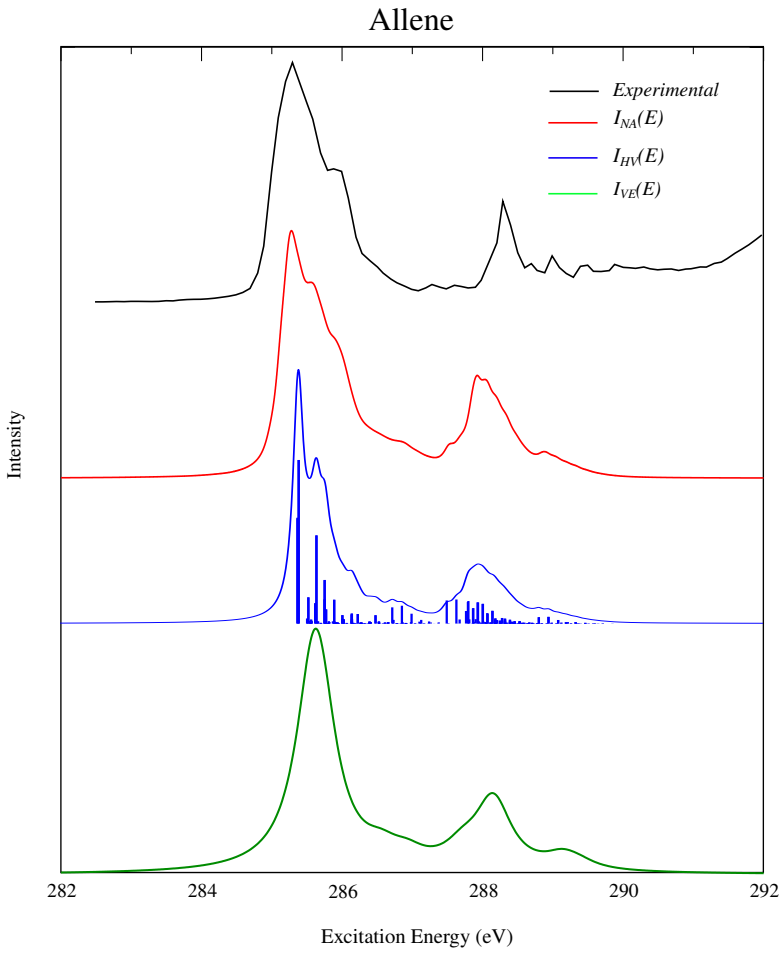

Figure S7. The experimental X-ray absorption of allene compared to simulations without shifting excitation energy of each core-excited state in the calculated spectra performed employing a hierarchy of approximations. From bottom, the I_{VE} is a purely electronic spectrum employing vertical excitation energies and oscillator strengths only (green line), I_{HV} is poisson distribution spectrum corresponding to vibrational structure arising from treating the excited states as a series of displaced harmonic oscillators (blue line), and I_{NA}, the full non-adiabatic vibronic coupling simulation (red line). The experimental spectrum is at top (black line). [7].

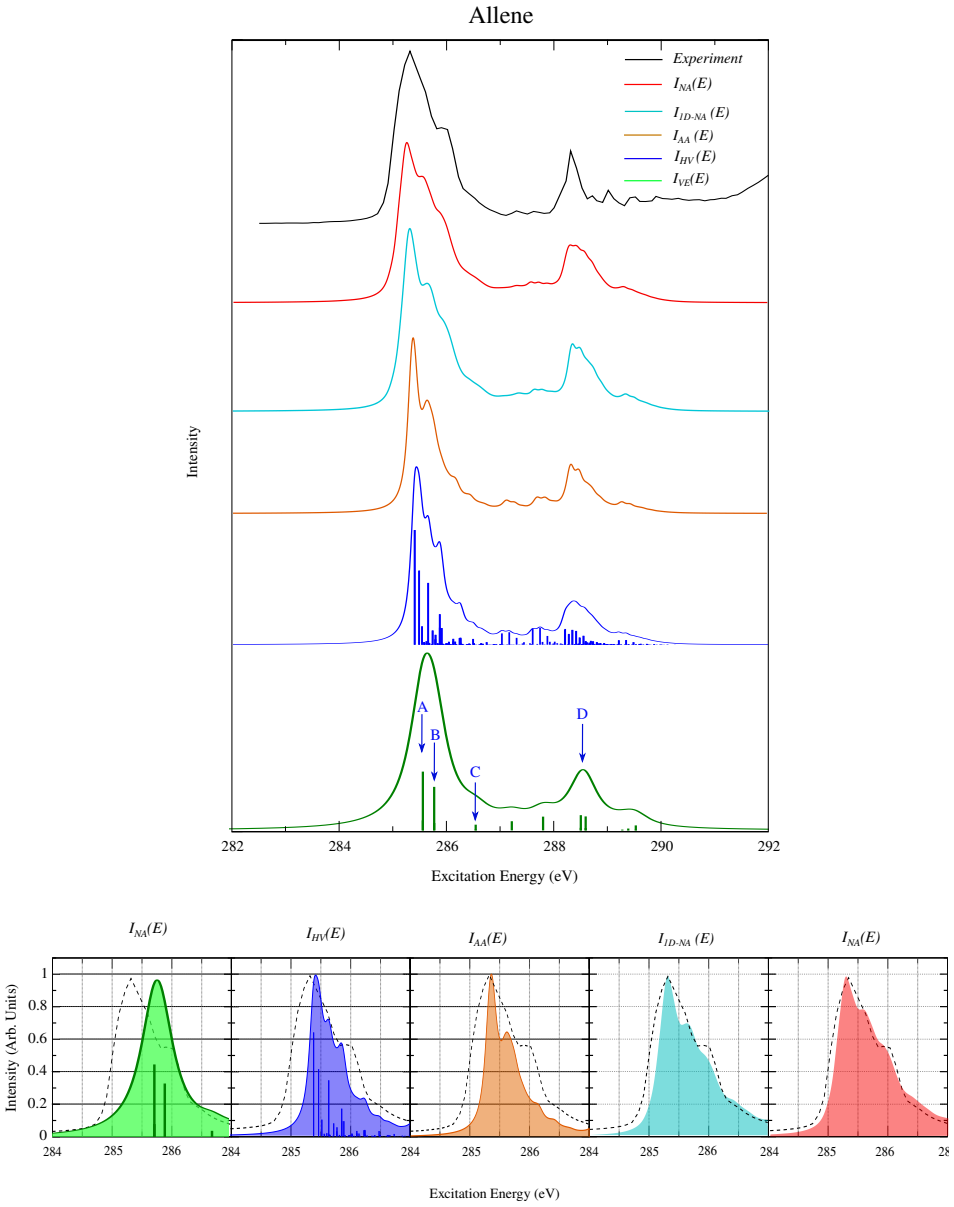

Figure S8. The experimental X-ray absorption of allene compared to simulations performed employing a hierarchy of approximations. From bottom, the I_{VE} is a purely electronic spectrum employing vertical excitation energies and oscillator strengths only (green line), I_{HV} is Poisson distribution spectrum corresponding to vibrational structure arising from treating the excited states as a series of displaced harmonic oscillators (blue line), I_{AA}, the vibronic coupling Hamiltonian model considering only one-mode terms for the diabatic potential and all interstate couplings were switched off (orange line), I_{1D-NA}, the vibronic coupling Hamiltonian model considering only one-mode terms for the diabatic potential and inter-state coupling terms, and I_{NA}, the full non-adiabatic vibronic coupling simulation (red line). The experimental spectrum is at top (black line). [7]. The bottom panels evince a detailed comparison of the various approximations with the experimental band origin.

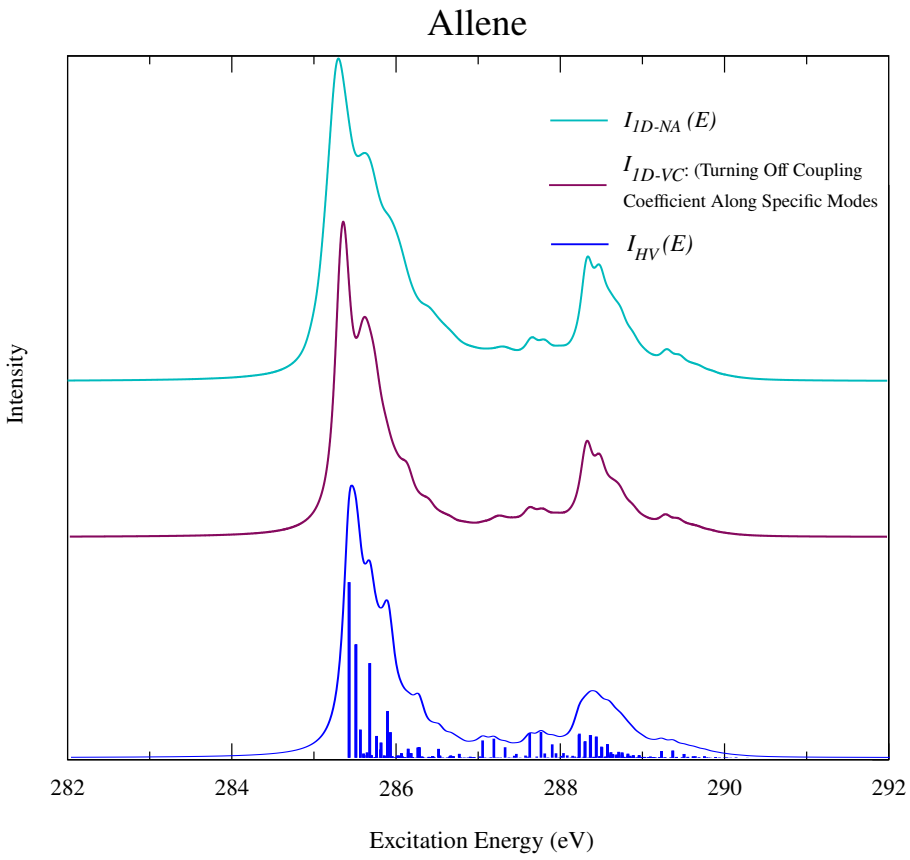

Figure S9. Simulated X-ray absorption spectra of allene performed employing a hierarchy of approximations. From bottom, I_{HV} is poisson distribution spectrum corresponding to vibrational structure arising from treating the excited states as a series of displaced harmonic oscillators (blue line), I_{1D-VC}, the vibronic coupling Hamiltonian model considering only one-mode terms for the diabatic potential and inter-state coupling terms turning off inter-state coupling coefficients along modes Q1, Q2 and Q5(maroon line), and I_{1D-VC}, the vibronic coupling Hamiltonian model considering only one-mode terms for the diabatic potential and inter-state coupling terms (cyan line).

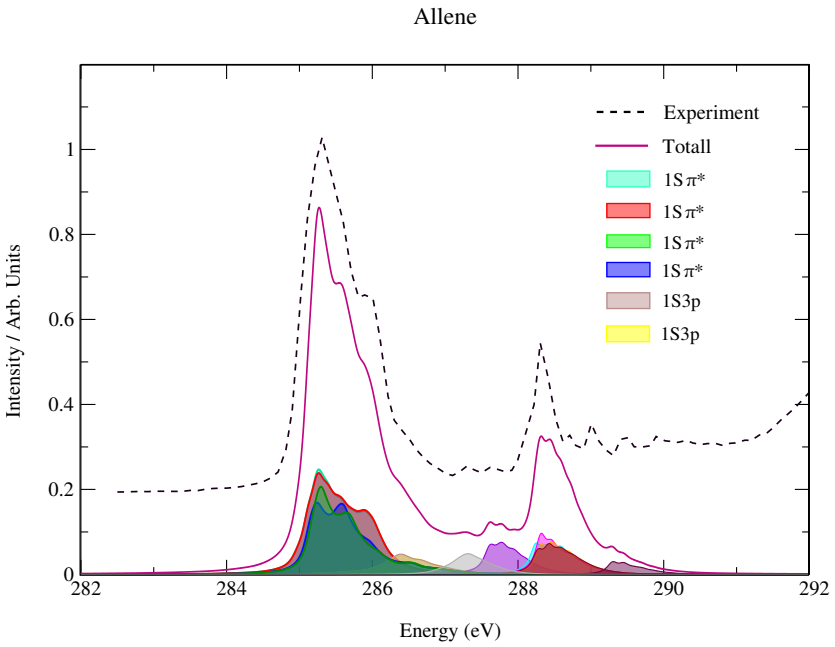

Figure S10. Vibronic absorption spectra of allene including individual state component computed using vibronic coupling Hamiltonians parameterized via fitting to quasi-diabatic potentials computed at the QD-DFT/MRCI(2) levels of theory using the aug-cc-pVTZ basis.

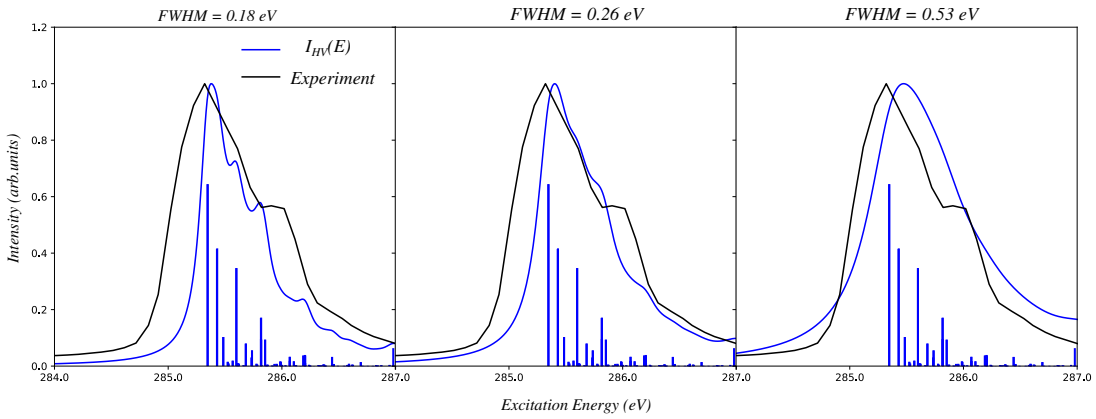

Figure S11. Comparison of the allene $I_{HV}(E)$ spectra at the band origin obtained with different Lorentzian broadening values.

Butadiene

Geometry and Normal Modes

```
Geometry information of Butadiene

C      0.0002840     0.7265345     0.0000000
C     -0.0002840    -0.7265345     0.0000000
C      1.1026055     1.4789691     0.0000000
C     -1.1026055    -1.4789691     0.0000000
H     -0.9728538     1.2088423     0.0000000
H      0.9728538    -1.2088423     0.0000000
H      1.0522871     2.5589403     0.0000000
H      2.0903284     1.0337469     0.0000000
H     -1.0522871    -2.5589403     0.0000000
H     -2.0903284    -1.0337469     0.0000000
```

States	Computed f_i	Adjusted f_i	Computed E_i^0 (eV)	Energy Shifts (eV)
$1A_u$	0.0997	0.0997	284.73	-0.3
$2A_u$	0.0840	0.0714	285.36	-0.3
$1B_u$	0.0102	0.0204	286.96	0.2
$2B_u$	0.0300	0.0600	287.33	0.2
$3B_u$	0.0110	0.0220	287.54	0.2
$4B_u$	0.0028	0.0056	287.55	0.2
$3A_u$	0.0008	0.0008	287.88	0.2
$5B_u$	0.0041	0.0041	287.94	0.2
$6B_u$	0.0011	0.0011	288.18	0.2
$4A_u$	0.0130	0.0130	288.25	0.2
$7B_u$	0.0065	0.0065	288.28	0.2
$8B_u$	0.0045	0.0045	288.30	0.2
$5A_u$	0.0060	0.0060	288.39	0.2

Table S6. Computed and adjusted oscillator strengths (f_i) for butadiene, along with the applied energy shifts. The computed values are obtained from electronic structure calculations, while the adjusted values are modified to improve agreement with experimental spectra. The Energy Shifts column reflects the applied corrections to the computed excitation energies, yielding empirically informed theoretical best estimates of the vertical excitation energies (ϵ_{0i}).

normal mode	Operator File Label
$Q1$	$Q23$
$Q2$	$Q22$
$Q3$	$Q19$
$Q4$	$Q18$
$Q5$	$Q16$
$Q6$	$Q13$
$Q7$	$Q12$
$Q8$	$Q6$
$Q9$	$Q23$
$Q10$	$Q11$
$Q11$	$Q8$
$Q12$	$Q4$
$Q13$	$Q1$
$Q14$	$Q9$
$Q15$	$Q7$
$Q16$	$Q5$
$Q17$	$Q24$
$Q18$	$Q21$
$Q19$	$Q20$
$Q20$	$Q17$
$Q21$	$Q15$
$Q22$	$Q14$
$Q23$	$Q10$
$Q24$	$Q2$

Table S7. Mapping of normal mode labels used in the operator files of butadiene.

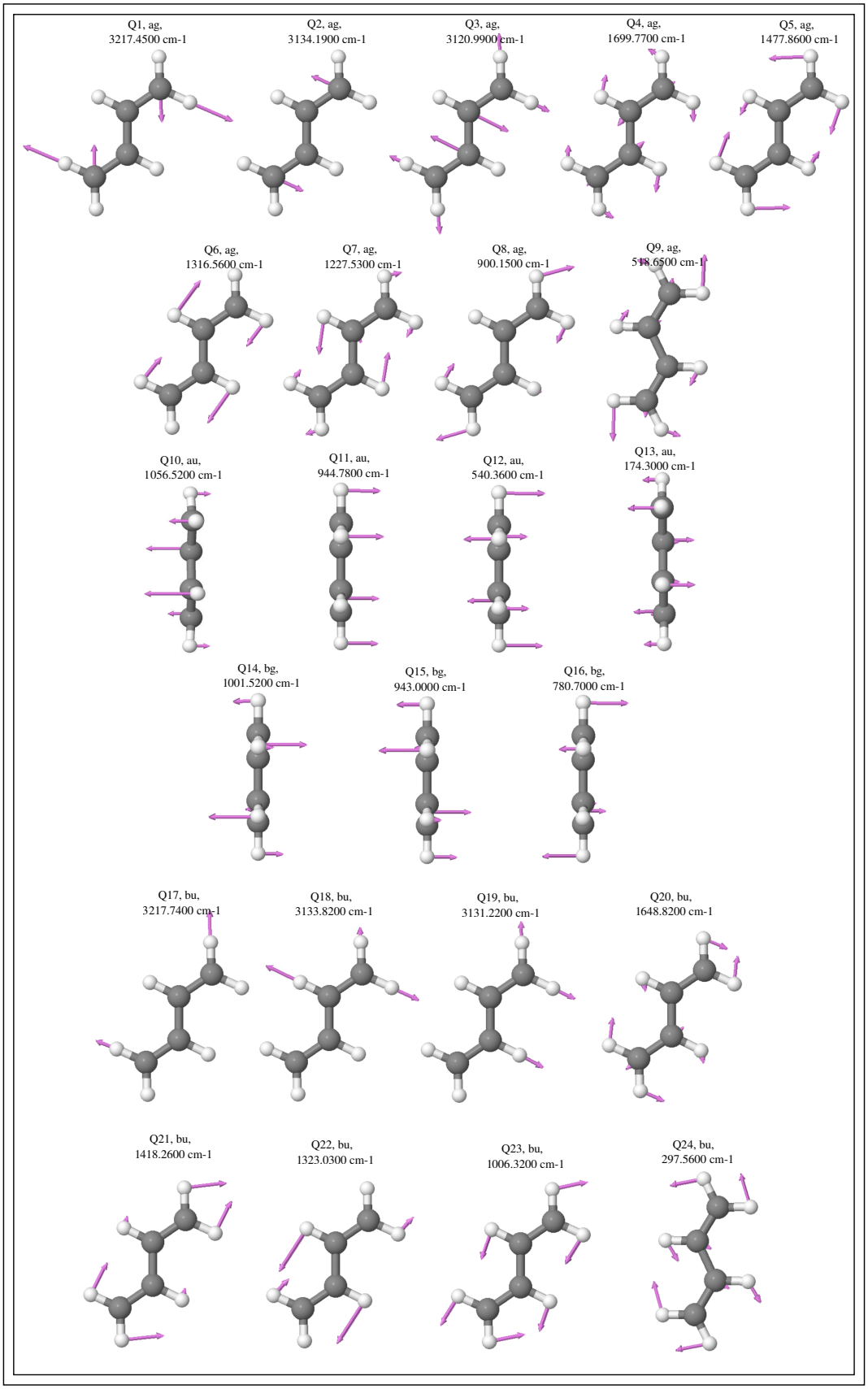

Figure S12. Vibrational normal modes of butadiene.

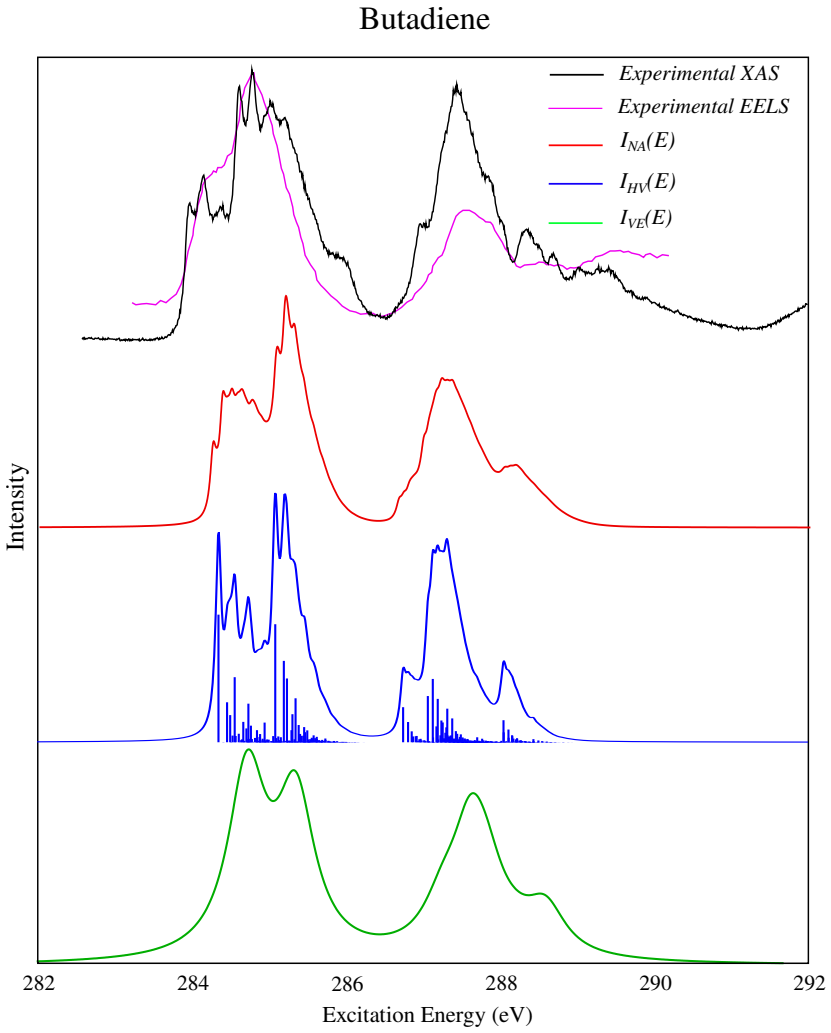

Figure S13. The experimental X-ray absorption of butadiene compared to simulations without shifting excitation energy of each core-excited state in the calculated spectra performed employing a hierarchy of approximations. From bottom, the I_{VE} is a purely electronic spectrum employing vertical excitation energies and oscillator strengths only (green line), I_{HV} is poisson distribution spectrum corresponding to vibrational structure arising from treating the excited states as a series of displaced harmonic oscillators (blue line), and I_{NA}, the full non-adiabatic vibronic coupling simulation (red line). The experimental XAS spectrum (black line) [7]) and EELS spectrum (magenta line) [12] are at top.

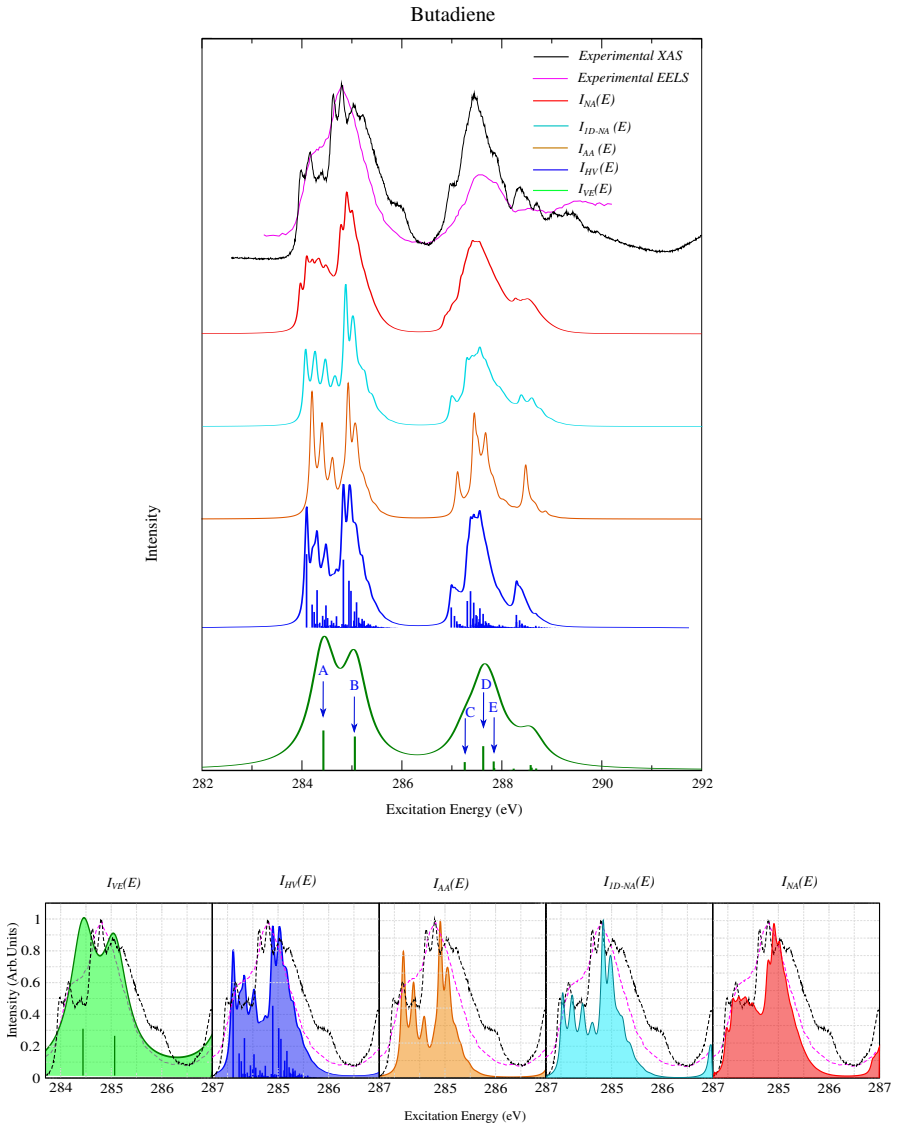

Figure S14. The experimental X-ray absorption of butadiene compared to simulations performed employing a hierarchy of approximations. From bottom, the I_{VE} is a purely electronic spectrum employing vertical excitation energies and oscillator strengths only (green line), I_{HV} is Poisson distribution spectrum corresponding to vibrational structure arising from treating the excited states as a series of displaced harmonic oscillators (blue line), I_{AA}, the vibronic coupling Hamiltonian model considering only one-mode terms for the diabatic potential and all interstate couplings were switched off (orange line), I_{1D-NA}, the vibronic coupling Hamiltonian model considering only one-mode terms for the diabatic potential and inter-state coupling terms, and I_{NA}, the full non-adiabatic vibronic coupling simulation (red line). The experimental XAS spectrum (black line) [7]) and EELS spectrum (magenta line) [12] are at top. The bottom panels evince a detailed comparison of the various approximations with the experimental band origin.

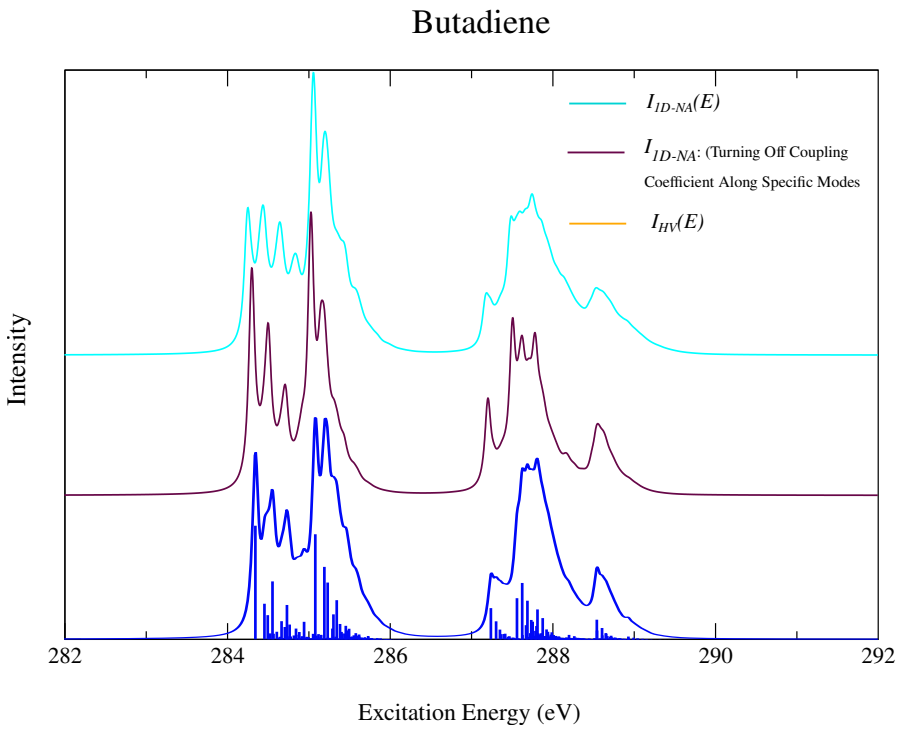

Figure S15. Simulated X-ray absorption spectra of butadiene performed employing a hierarchy of approximations. From bottom, I_{HV} is poisson distribution spectrum corresponding to vibrational structure arising from treating the excited states as a series of displaced harmonic oscillators (blue line), I_{1D-VC}, the vibronic coupling Hamiltonian model considering only one-mode terms for the diabatic potential and inter-state coupling terms turning off inter-state coupling coefficients along modes Q2, Q14, Q17, Q20 and Q21(maroon line), and I_{1D-VC}, the vibronic coupling Hamiltonian model considering only one-mode terms for the diabatic potential and inter-state coupling terms (cyan line).The black curve is the experimental spectrum shown for comparison [7].

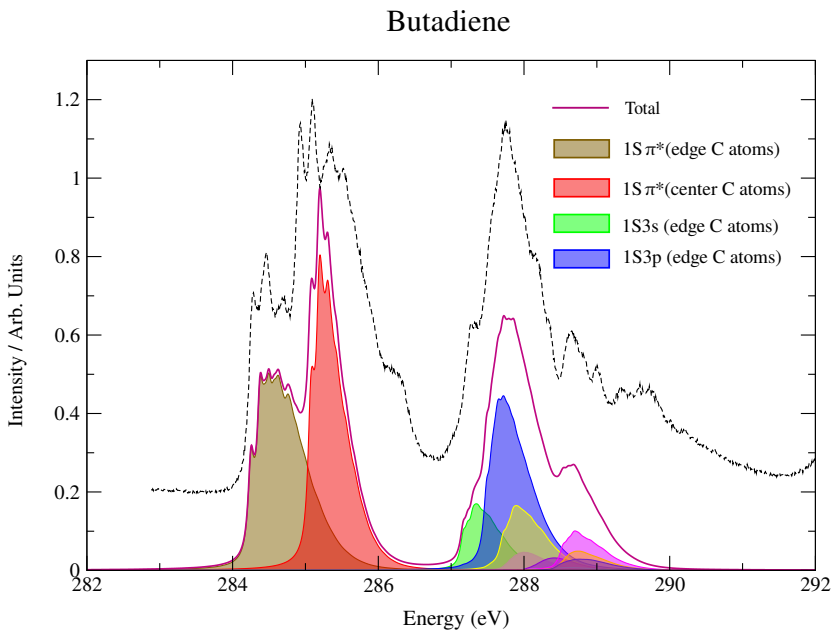

Figure S16. Vibronic absorption spectra computed of butadiene including individual state component using vibronic coupling Hamiltonians parameterized via fitting to quasi-diabatic potentials computed at the QD-DFT/MRCI(2) levels of theory using the aug-cc-pVTZ basis.

* Michael.Schuurman@uottawa.ca

[1] Beck, M. H., Jäckle, A., Worth, G. A., and Meyer, H.-D. The multiconfiguration time-dependent hartree (mctdh) method: a highly efficient algorithm for propagating wavepackets. *Physics reports 324*, 1 (2000), 1–105.

[2] Bowman, J. M. *Vibrational dynamics of molecules*. World Scientific, 2022.

[3] Dirac, P. A. Note on exchange phenomena in the thomas atom. In *Mathematical proceedings of the Cambridge philosophical society* (1930), vol. 26, Cambridge University Press, pp. 376–385.

[4] Ehara, M., Meyer, H.-D., and Cederbaum, L. Multiconfiguration time-dependent hartree (mctdh) study on rotational and diffractive inelastic molecule-surface scattering. *The Journal of chemical physics 105*, 19 (1996), 8865–8877.

[5] Fielding, H. H., and Worth, G. A. Using time-resolved photoelectron spectroscopy to unravel the electronic relaxation dynamics of photoexcited molecules. *Chemical Society Reviews 47*, 2 (2018), 309–321.

[6] Frenkel, J. Wave mechanics, clarendon, 1934.

[7] Ingle, R., Banerjee, A., Bacellar, C., Barillot, T., Longetti, L., Coreno, M., De Simone, M., Zuccaro, F., Poletto, L., Miotti, P., et al. Carbon k-edge x-ray emission spectroscopy of gas phase ethylenic molecules. *Journal of Physics B: Atomic, Molecular and Optical Physics 55*, 4 (2022), 044001.

[8] Manthe, U. A multilayer multiconfigurational time-dependent hartree approach for quantum dynamics on general potential energy surfaces. *The Journal of chemical physics 128*, 16 (2008).

[9] Manthe, U., Meyer, H.-D., and Cederbaum, L. S. Wave-packet dynamics within the multiconfiguration hartree framework: General aspects and application to nocl. *The Journal of chemical physics 97*, 5 (1992), 3199–3213.

[10] Meyer, H.-D., Gatti, F., and Worth, G. A. *Multidimensional quantum dynamics: MCTDH theory and applications*. John Wiley & Sons, 2009.

[11] Meyer, H.-D., Manthe, U., and Cederbaum, L. S. The multi-configurational time-dependent hartree approach. *Chemical Physics Letters 165*, 1 (1990), 73–78.

[12] Sodhi, R. N., and Brion, C. High resolution carbon 1s and valence shell electronic excitation spectra of trans-1,3-butadiene and allene studied by electron energy loss spectroscopy. *Journal of Electron Spectroscopy and Related Phenomena 37*, 1 (1985), 1–21.

[13] Vendrell, O., and Meyer, H.-D. Multilayer multiconfiguration time-dependent hartree method: Implementation and applications to a henon–heiles hamiltonian and to pyrazine. *The Journal of Chemical Physics 134*, 4 (2011), 044135.

[14] Wang, H. Multilayer multiconfiguration time-dependent hartree theory. *The Journal of Physical Chemistry A 119*, 29 (2015), 7951–7965.

[15] Wang, H., and Thoss, M. Multilayer formulation of the multiconfiguration time-dependent hartree theory. *The Journal of chemical physics 119*, 3 (2003), 1289–1299.

[16] Worth, G. Quantics: A general purpose package for quantum molecular dynamics simulations. *Computer Physics Communications 248* (2020), 107040.

[17] Worth, G. A., Meyer, H.-D., and Cederbaum, L. Relaxation of a system with a conical intersection coupled to a bath: A benchmark 24-dimensional wave packet study treating the environment explicitly. *The Journal of chemical physics 109*, 9 (1998), 3518–3529.